Optical Power-Electronic Technology

S.K. Mazumder, *Sr. Member, IEEE,* A. Mojab, H. Riazmontazer, S. Mehrnami, *Student Members, IEEE*

***Abstract*— In this paper, a top-level outline on the work related to optically-switched power semiconductor devices that have been carried out at the University of Illinois, Chicago (UIC) or those in which UIC has been involved has been outlined. In addition, an outline on optical control that affects the switching dynamics of the power semiconductor devices is provided.**

Disclaimer: This paper emulates an earlier paper published by the authors with the following description and is reproduced here primarily for further visibility and educational outreach: S.K. Mazumder, A. Mojab, and H. Riazmontazer, "Optically-switched wide-bandgap power semiconductor devices and device-transition control," Physics of Semiconductor Devices: 17th International Workshop on the Physics, Springer, pp. 57–65, 2013. This work is supported in part by U.S. NSF (award no. 1202384) and U.S. ARPA-E (award no. DE-AR0000336). However, any opinions, findings, conclusions, or recommendations expressed herein are those of the authors and do not necessarily reflect the views of the NSF or ARPA-E.

I. Introduction

OPTICALLY-triggered power semiconductor devices provide some major advantages over their electrically-triggered counterpart. Such advantages are multi-fold and encompass a) immunity to electromagnetic interference, b) elimination of back-propagation effect from the power stage to the control stage, c) higher reliability due to complete electrical isolation, d) simple realization of gate drive for high power multilevel and series connected device based power-conversion systems, and e) easy controllability of switching dynamics thereby enabling systems control at the device level to name a few. As such, the potential applications of such optically-triggered power semiconductor devices include fly-by-light (FBL), smart grid, electric vehicles, power-quality conditioners, renewable energy, electromechanical launch systems, and pulsed-power systems. Another application of such a technology is the ability to control the switching dynamics of both electrically- and optically-triggered power semiconductor devices thereby enabling systems control at device level with regard to several performance and reliability parameters including dv/dt and di/dt stress, switching loss, as well as noise mitigation.

II. Overview of Previously Achievements on the Optical Power Semiconductors

A. Optically-Triggered Power Transistor (OTPT) [1]

Our research on optically-triggered power semiconductor switches initiated with a lateral GaAs-based optically-triggered power transistor (OTPT). GaAs has a high level of light absorption and hence a high quantum efficiency. Fig. 1 shows the device structure of the GaAs-based OTPT, micrograph of a prototype OTPT and its packaged realization [1]. The OTPT has a lateral structure with two electrodes: collector and emitter. N-drift, P-base, and N+ collector regions are grown using MOCVD technique. Shallow low-energy Si-ion implanted N^+ regions make the contacts between the emitter electrode and the semiconductor. Optical window is defined by the Si_3N_4 anti-reflecting layer of a particular thickness, which results in minimum reflection of light. In the blocking state, the applied voltage is supported by the reverse biased P-N junction between the P-base and N-drift regions. In Fig. 2, 3-D diagrams of electric-field distribution and photogeneration rate across the device in

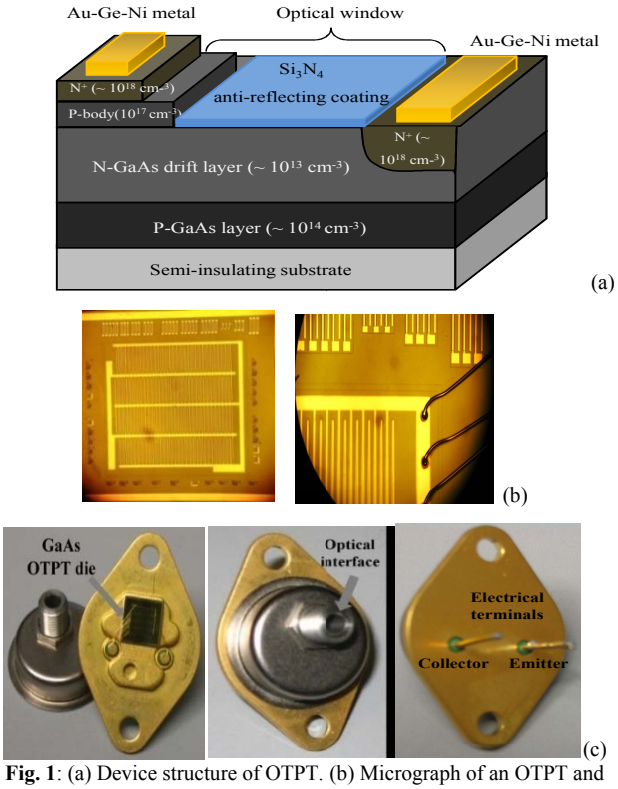

Fig. 1: (a) Device structure of OTPT. (b) Micrograph of an OTPT and its die wire bonding. (c) Packaged realization of the OTPT [1].

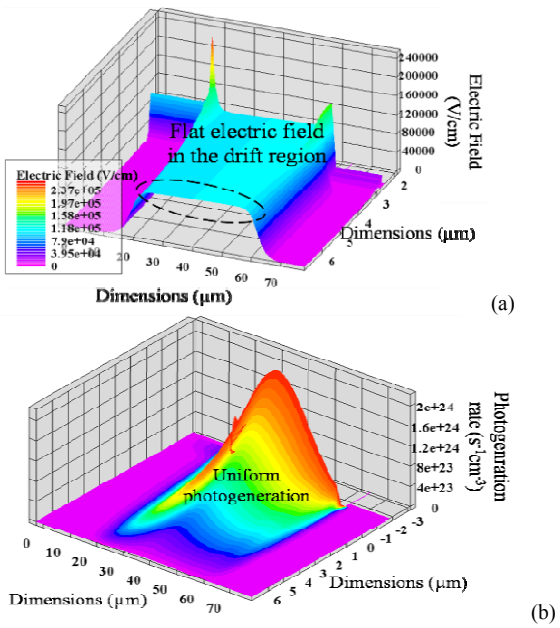

Fig. 2: (a) Three-dimensional view of the electric-field distribution inside the OTPT at the instant of breakdown. (b) Three-dimensional view of the uniform photogeneration rate inside the OTPT [1].

978-1-4799-5115-4/14/$31.00 ©2014 IEEE

Fig. 1a is shown. This rectangular electric field enables reduced effective distance between collector and emitter electrodes of the unit cell of the OTPT and yields higher optical gain, because photogenerated carriers travel less distance inside N-drift region. Also, a rectangular electric field (Fig. 2a) mobilizes the photogenerated carriers in a uniform manner, as demonstrated in Fig. 2b. The quantum efficiency and the switching speed of the OTPT depend strongly on the minority-carrier recombination lifetime in the P-body region. A higher doping of the P-body results in a shorter lifetime, which ensures faster turn-off due to rapid recombination when the light shuts off, but, it also leads to a lower device gain because photogenerated carriers recombine easily and have less chance of contributing towards conductivity modulation. The on-state resistance of the OTPT, varies with the optical intensity as shown in Fig. 3.

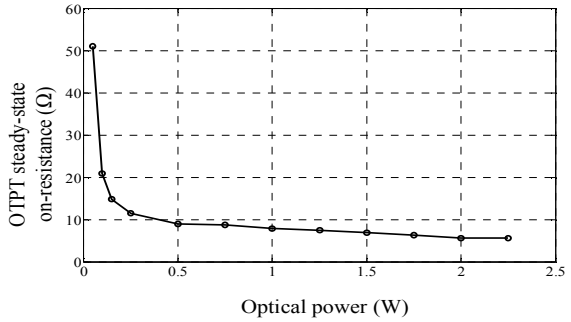

Fig. 3: Experimental OTPT on-resistance with varying optical power under the following conditions: V_{Bias} = 10 V, R_{load} = 50 Ω, frequency = 5 kHz, and duty cycle = 50% [1].

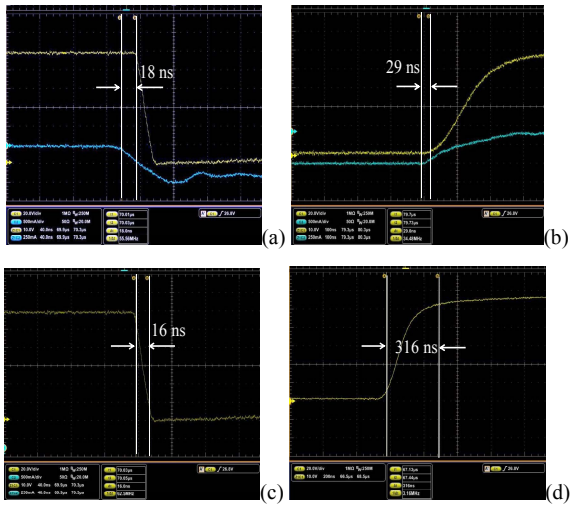

Fig. 4: A snapshot of the (a) turn-on delay, (b) turn-off delay, (c) rise time and (d) fall time of the OTPT under the following conditions: V_{Bias} = 60 V, R_{load} =1000 Ω, frequency = 50 kHz, duty cycle = 50%, and optical power = 0.5 W. Scale for the vertical axis is 10 V/div while for the horizontal axes are : (a) 40 ns/div, (b) 100 ns/div, (c) 40 ns/div, and (d) 200 ns/div, respectively. For (a) and (b), the top trace is the voltage across the OTPT and the bottom trace is the output current signal of the laser driver. The laser-driver current signal is measured through an internal current monitor of the laser-driver and is of negative polarity. The threshold current, at which the lasing starts, is ~ 6 A [1].

Snapshots of the turn-on and turn-off dynamics of the OTPT are shown in Fig. 4. Turn-on and turn-off delays are measured as the difference between the time instants of the initiation of the laser-drive signal and initiation of the change in the OTPT voltage. Rise and fall times are defined as the time taken to change the OTPT voltage from 10% to 90% (or vice versa) of its steady-state value.

Subsequently, attempt was made to integrate the OTPT as a driver for a set of higher-voltage power semiconductor devices to realize optically-triggered hybrid power devices. In Fig. 5, the schematic diagram of one such hybrid package and the tested prototype package is shown. The aim of such hybrid packaging is to reduce the interconnect length to minimize the parasitic impedance between the OTPT(s) and the PSD due to interconnects.

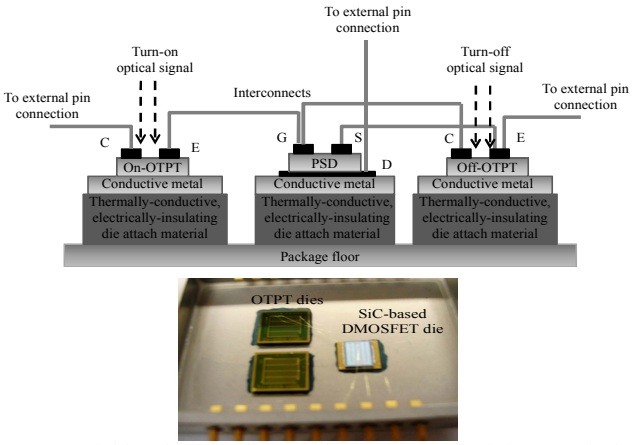

Fig. 5: Hybrid packaging scheme with two OTPTs coupled to a vertical PSD die. Corresponding prototype package is shown where the PSD die is SiC-based MOSFET. Electrical terminals are indicated by the symbols G, D, S, C, and E that represent gate, drain, source, collector, and emitter, respectively [1].

The concept of OT hybrid power semiconductor device was tried using a combination of triggering OTPT(s) and high-voltage devices such as SiC MOSFET, SiC VJFET, Si IGBT, Si MOSFET devices. Fig. 6 [1] shows the transient performance of such optical hybrid devices.

B. Vertical Optically-Triggered Power Transistor

More recently, a vertical OTPT based on Si has been designed, fabricated, and characterized that can support much higher current of operation and fast switching dynamics. The device is designed to support a junction temperature of 200 ^{o}C. Even though the initial goal of the OTPT is to support the function of Q1 in Fig. 12 that represents an optically-triggered emitter turn-off thyristor, the vertical OTPT can be used independently and for other hybrid configurations. Figs. 7 and 8 demonstrate the information regarding the OTPT.

C. Optically-Triggered SiC GTO Thyristor [2],[3]

The GaAs-based OTPTs described in Section II were used along with a SiC GTO [3]. The device structure and fabricated prototype of a SiC GTO is shown in Fig. 9 along with switching results in Fig. 10. The optically-triggered GTO is also shown in Fig. 11. Two different bias voltages are applied to the gate of the thyristor by using the OTPTs. This voltages force the thyristor to turn on and off. An important advantage of using optical switches in GTO structure is removing the effect of electromagnetic interference (EMI) in the low-power parts of the GTO. The simulation results showing the switching capability of this proposed optically-triggered GTO is given in Fig. 10.

D. A New Single-Biased All-Optically Triggered Configuration for ETO Thyristor [4]

ETOs are one of the most promising devices in very high voltage fast switching power electronic applications.

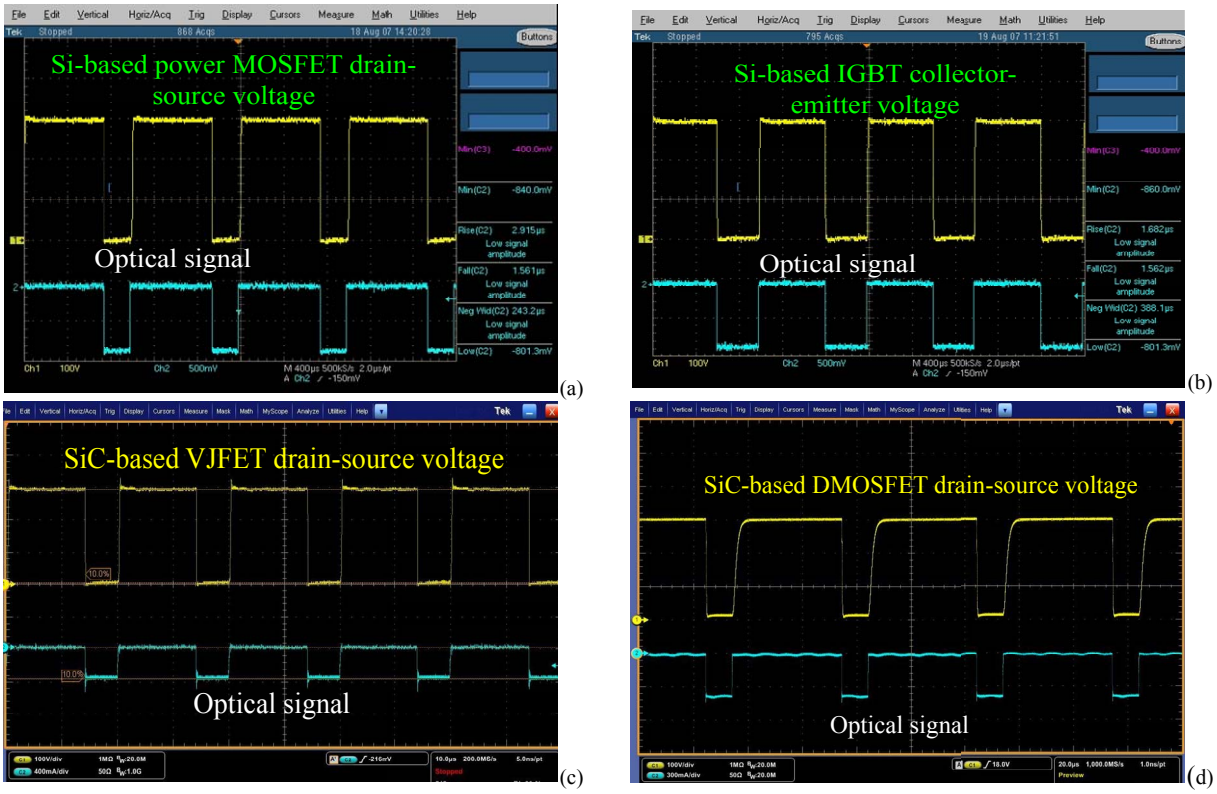

Fig. 6: Nominal switching operation for the OTPT(s) coupled to different types of power semiconductor devices [1]: (a) Si-based power MOSFET (CoolMOS part number 47N50), (b) Si-based IGBT (IRG4CC50), (c) 600 V normally-on SiC-based VJFET, and (d) 600 V SiC-based DMOSFET. The dynamics of the SiC DMOSFET is comparatively slower due to the high input capacitance of the device and is not attributed to the OTPT.

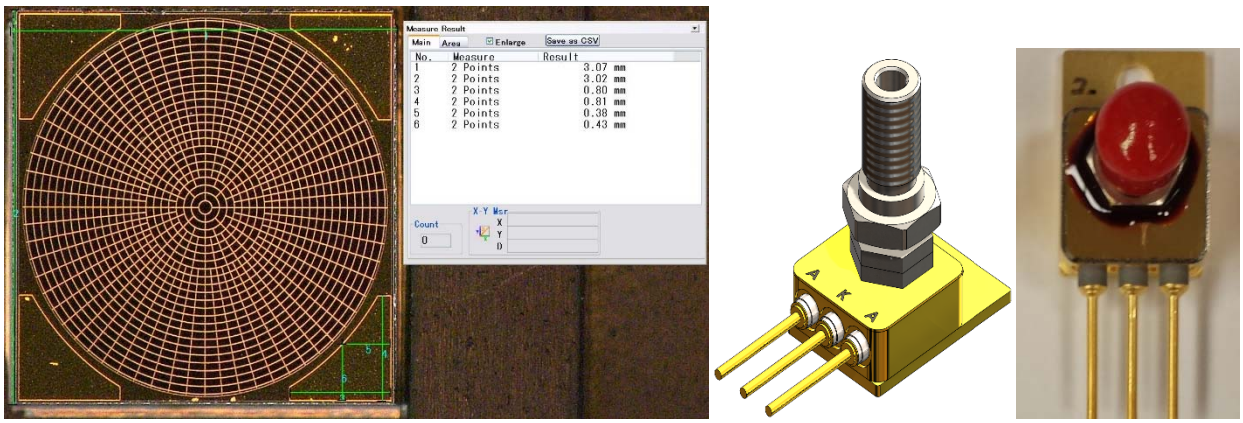

Fig. 7: Vertical experimental OTPT device geometry, packaging architecture and actual package.

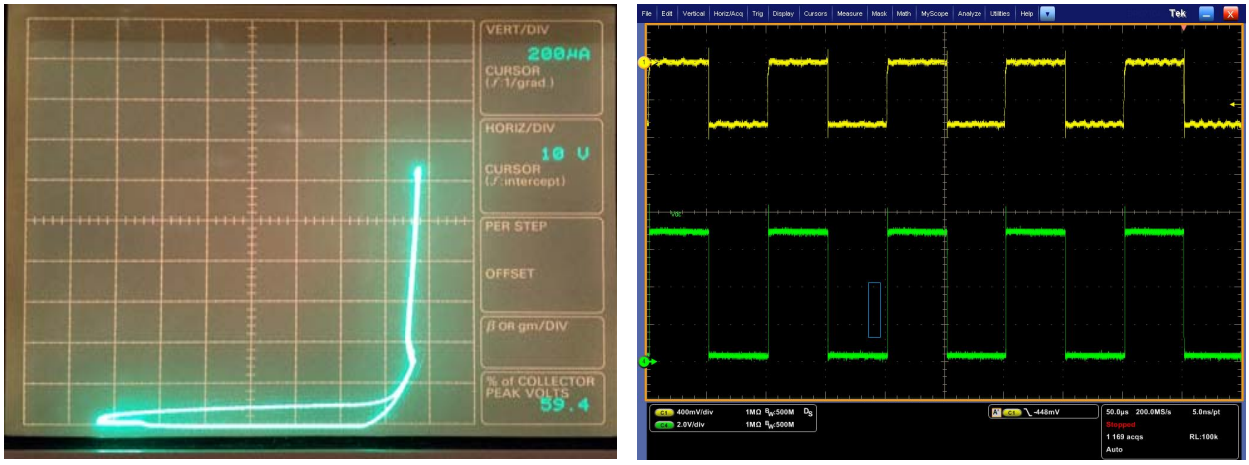

Fig. 8: Experimental I-V and switching characterization of the vertical OTPT.

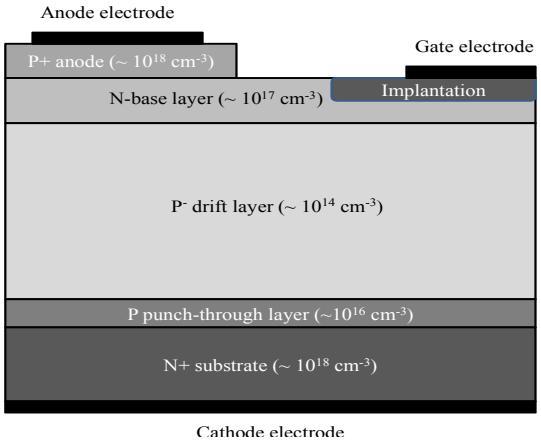

(a)

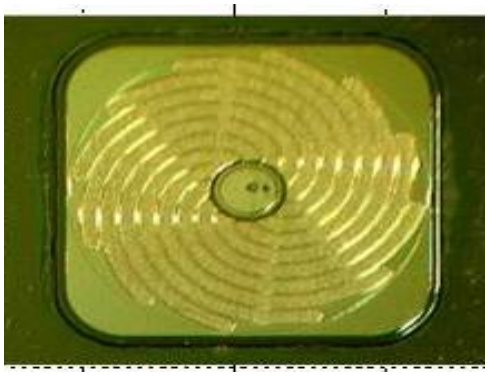

(b)

Fig. 9: (a) SiC GTO structural schematic and (b) fabricated prototype

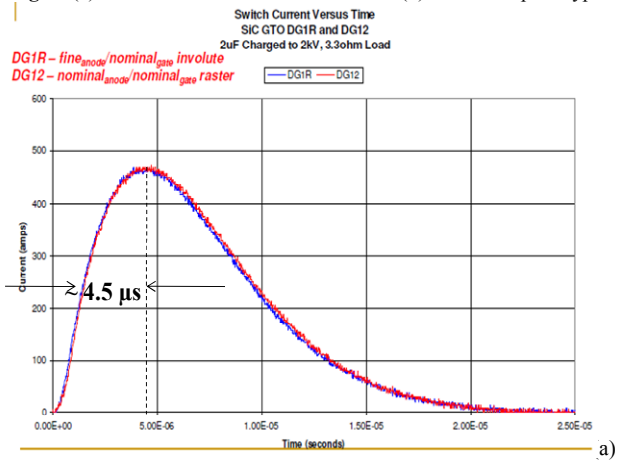

a)

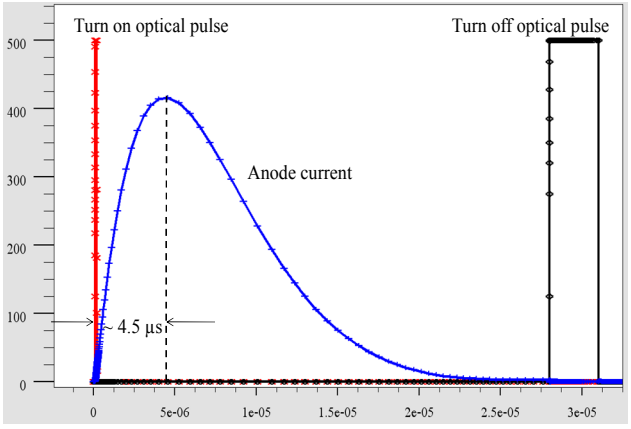

(b)

Fig. 10: Switching result of the SiC GTO with $V_{cathode}$ = - 2000 V, C_{charge} = 2 μF, R_{load} = 3.3 Ω, (a) experimental result with electrical gate triggering and (b) simulation result with optical triggering using GaAs OTPTs.

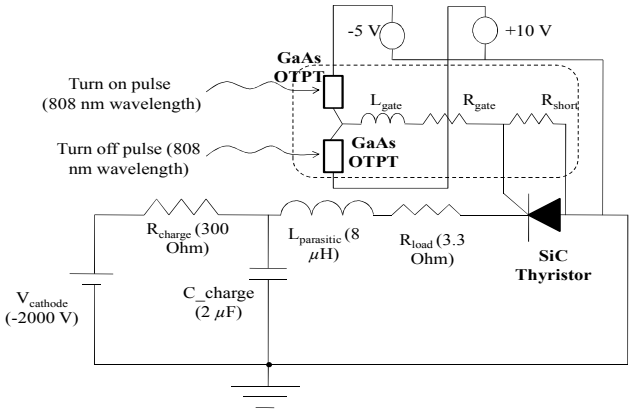

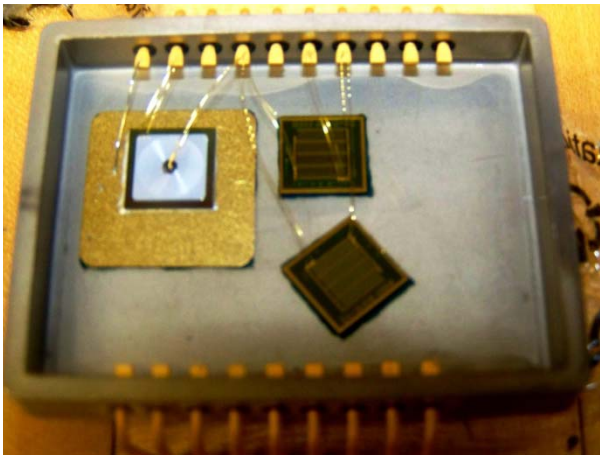

Fig. 11: Schematic of the switching simulation circuit for optically-controlled SiC GTO [2].

The novel single-biased all-optically triggered ETO is shown in Fig 12. The device structure of the SiC thyristor is shown in Fig. 13. Here an optically-gated thyristor is used. More details about the all-optical ETO, optical thyristor and its manufacturing process are given in [5], [6]. The laser light is exposed directly to the n-type gate region of the thyristor; furthermore, the depletion region is highly expanded across the main blocking p-n junction between the gate and drift layers. So the gate layer plays an important role in absorbing light and determining the

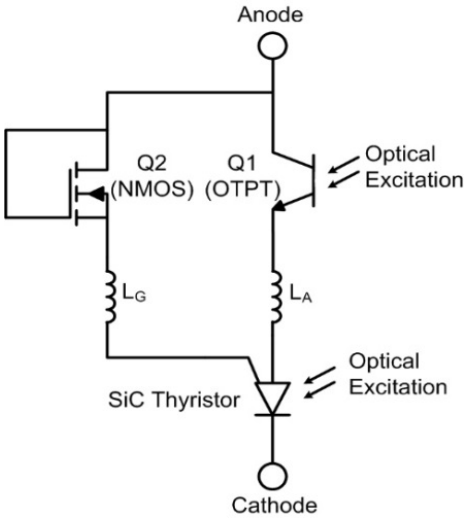

Fig. 12: Structure of the hybrid all-optical ETO. L_G and L_A represent the packaged parasitic inductance.

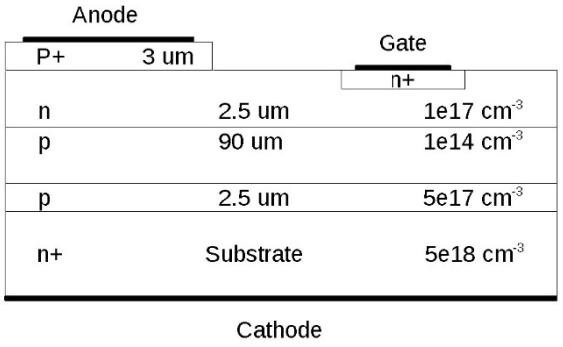

Fig. 13: Structure of the optical SiC thyristor [4].

thyristor breakdown voltage. Since the built-in potential of the top p-n layers of the main thyristor is about 3 V, we used an NMOSFET with high threshold voltage to prevent it from conducting in the on-state.

A schematic diagram of the OTPT used in the ETO configuration in Fig. 12 is shown in Fig. 14. This optical device can be implemented on either Si or GaAs

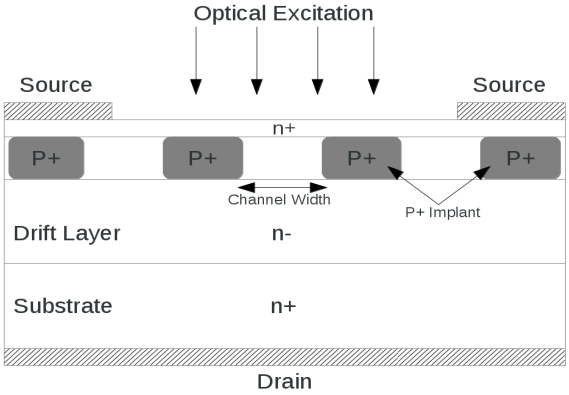

Fig. 14: Device structure for the OTPT of the optical ETO in Fig. 12.

substrates. The channel width of this device can be modulated according to the power of the exposed laser beam. Under dark conditions, the depletion layer from two adjacent p+ regions close the device channel and the high resistive mode is obtained. When illuminated, the channel opens according to the power of the light and the low resistive mode is obtained. An important advantage of this kind of optical switch, which makes it superior to other kinds of MOSFET-based switches, is the controlled conductivity upon the optical power.

The ETO turn-on process starts by illuminating both the OTPT and thyristor at the same time. Since SiC is a wide bandgap material with a bandgap of 3.23 eV, a laser beam with a wavelength of less than about 380 nm is required to trigger the SiC thyristor. Currently, we have used a 250-nm laser beam for the SiC thyristor and an 808-nm laser beam for the silicon-based OTPT.

The ETO turn-off procedure starts when the laser beam on the OTPT is removed. Subsequently, the resistance of the OTPT rises rapidly which leads to a rapid increase in the voltage across the NMOSFET. Once this voltage exceeds the threshold voltage of the NMOSFET, it starts to conduct. Then, all the current from the anode contact of the thyristor is commutated to the gate contact, forcing the thyristor to turn off rapidly under unity-gain condition.

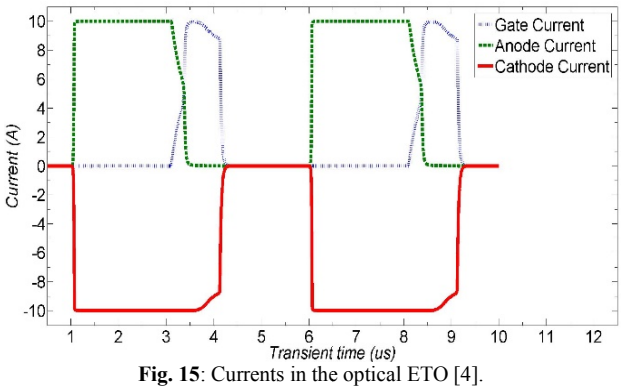

Fig. 15: Currents in the optical ETO [4].

Fig. 15 shows the results for the thyristor currents versus transient time for the optically-triggered ETO. The bias voltage and load current are 10 KV and 10 A respectively. A rise and fall time of 26 and 362 ns are achieved for the optically- triggered ETO. The on-state voltage drop of the OTPT was 0.15 V and the voltage drop across the thyristor was 4.2 V, leading to the total voltage drop of 4.4 V. This is roughly about 0.04% of the supply voltage. In the off state, a peak voltage of 5 V was applied to the OTPT, while at steady state a voltage of 2 V was applied, which is 0.02% of the total voltage.

III. Optically-Triggered Driver Based Transition Control of Power Semiconductor Devices

Once the OTPT in Fig. 1 was realized in fabrication, two such OTPTs were used along with a SiC MOSFET to form a hybrid optical package as shown in Fig. 16. The OTPTs Q1 and Q2 work oppositely and, respectively, turn-on and turn- off the SiC MOSFET. When the OTPT Q1 is illuminated, this OTPT goes to low resistivity condition and connects the gate of the SiC MOSFET to the bias voltage. Therefore, MOSFET (Q3) turns on rapidly, while there is no significant current passing through Q2. On the other hand, when the OTPT Q2 is illuminated and Q1 is off, the gate of SiC MOSFET is discharged through the path provided by Q2.

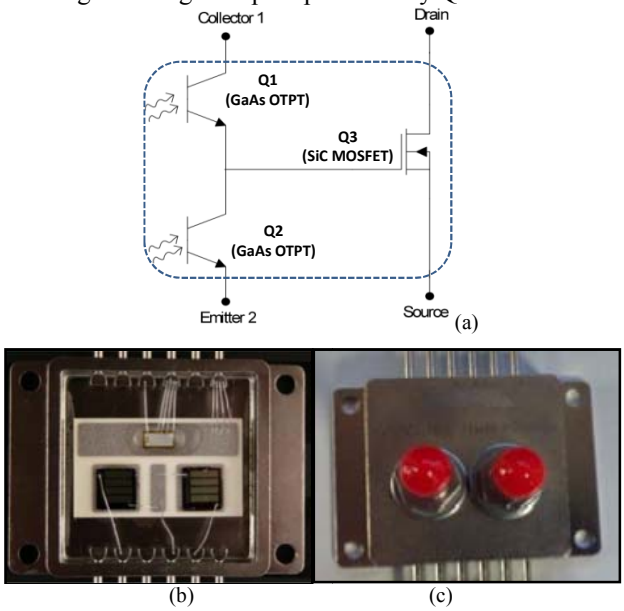

Fig. 16: Optically-controlled hybrid SiC device structure [7].

To verify the feasibility of the optical hybrid package at the converter level, it is used as the main switch in a buck converter. It has been shown in Fig. 17, that by

varying the optical intensity through OTPTs one is able to change the efficiency of the converter. As the optical power through the OTPTs increase the total switching transition duration increases, as the results switching loss decreases and efficiency increases. An initial sharp increment in the power-conversion efficiency is followed by a gradually saturating behavior. This shape is almost reciprocal to that observed in the variations of the OTPT on-resistance.

This optically-controlled driver was also used in a boost converter. The boost converter was tested up to an output of 250 W, feeding a 400 ohm low-inductance resistive load. The switching frequency was set at 0.25 MHz. The prototype and test results for boost converter are shown in Fig. 18 and Fig 19.

As indicated earlier, OTPTs can be placed in the charging and discharging path of the gate of an insulated gate power semiconductor device such as IGBT and MOSFET to modulate the turn-on and turn-off transitions by modulating the optical intensity to the optical window of the OTPTs. In the remaining section, initially the principle of optically-triggered switching-transition control is described. Subsequently, its implementation for MOSFET and IGBT is briefly illustrated. Finally, the experimental results are provided to support the theoretical explanations.

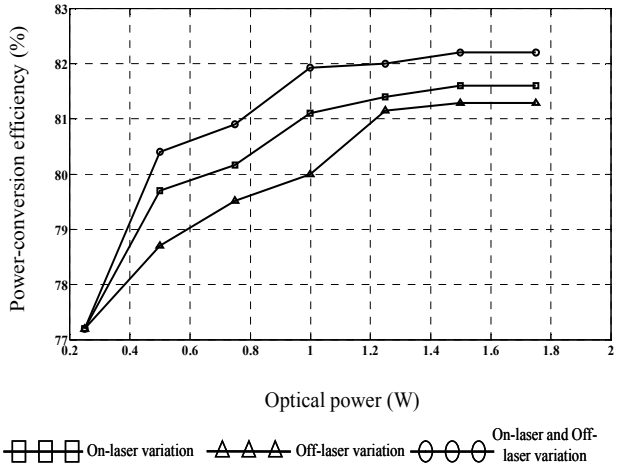

Fig. 17: Power-conversion efficiency of the buck converter with varying OTPT optical power and under the following conditions: V_{in} = 20 V, frequency = 100 kHz, duty cycle = 50%, R_{Load} = 2 Ω, and P_{load} = 50 W [1].

Fig. 18: Boost converter prototype showing OTPT-based optically-triggered packaged hybrid power device [7].

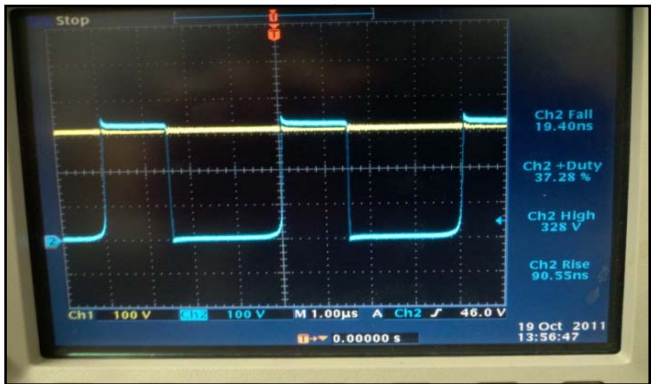

Fig. 19: Dc waveform shows the output of boost converter (328 V) and the pulsed waveform shows the drain to source voltage of the power MOSFET [7].

Turn-on and turn-off transients of the insulated-gate power semiconductor devices comprise a small portion of their switching operation period. However, these transients have a significant effect on the total switching loss which is a prominent part of the total loss of the converter. Furthermore, they have a direct effect on the conducted and radiated electromagnetic interference and device stresses such as peak overvoltage and peak reverse recovery current. Therefore, ability to control the switching transition is a pathway towards the total optimization in terms of loss, device stress and EMI. Furthermore, using the optical beam along with the OTPTs to modulate the switching transitions enables one to use a single beam of light to encode the PWM and intensity modulation signals and separate the control stage from the power stage.

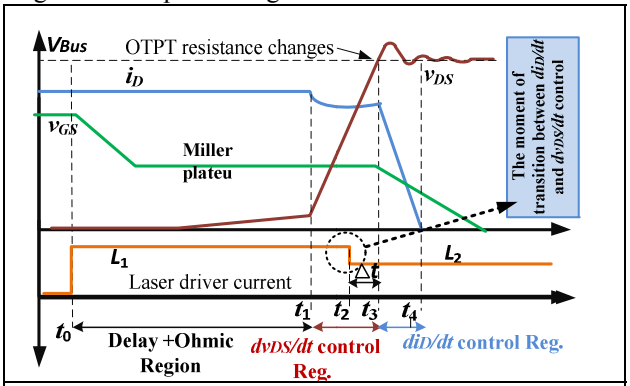

Fig. 20: Key waveforms of turn-off behavior of a power MOSFET.

The key waveforms of the turn-off transition of a SiC power MOSFET is shown in Fig. 20 [8]. The drain-to-source voltage slope (dv_{DS}/dt) in the dv_{DS}/dt control region shown in the Fig. 23 is approximated using:

$$dv_{DS}/dt \approx \frac{v_{GS,TH}+i_D/g_{fs}}{R_G C_{GD}} \quad (1)$$

where g_{fs} is the forward transconductance, i_D is the drain current, C_{GD} is the Miller capacitance, R_G is the gate resistance, and $v_{GS,TH}$ is the threshold voltage of MOSFET. The slope of the drain current (di_D/dt) in the di_D/dt control region shown in Fig. 23, is also approximated using:

$$di_D/dt \approx -\frac{V_{GS,TH}+i_D/2g_{fs}}{R_G C_{iss}/g_{fs}+L_\sigma} \quad (2)$$

In (2) C_{iss} is the input capacitance of a MOSFET and L_σ is the sum of parasitic inductances seen from the source

of MOSFET. Because of the parasitic inductances in the commutation path, di_D/dt in this region directly affects the overvoltage stress. According to (1) and (2), dv_{DS}/dt, di_D/dt and voltage overshoot and oscillation in the turn-on transition can be controlled by controlling the gate resistance of the MOSFET which in turn can be controlled by modulating the optical intensity to the OTPT which is placed in the discharging path of the gate of MOSFET.

Similarly, the key waveforms of the turn-on transition of an IGBT are shown in Fig. 21. Similar to the MOSFET's case, the slope of the collector current (di_C/dt) and slope of collector-to-emitter voltage (dv_{CE}/dt) in the turn-on transition are, respectively, approximated using (3) and (4):

$$\frac{di_C}{dt} \approx \frac{V_{CC}-V_{GET}-I_{L0}/g_m}{R_G.C_{GE}/g_m+L_\sigma} \quad (3)$$

$$\frac{dv_{CE}}{dt} \cong -\frac{V_{CC}-V_{GET}-I_{L0}/g_m}{R_G.C_{GC}} \quad (4)$$

In (3) and (4) V_{CC} represents the maximum gate voltage, V_{GET} represents the threshold voltage of IGBT, g_m is the forward trans-conductance of IGBT, C_{GE} is the gate-to-emitter capacitance, C_{GC} is the gate-to-collector capacitance, and I_{L0} is the load current of IGBT. di_C/dt of IGBT has a direct effect on the reverse recovery current of free-wheeling diode and current overshoot of the IGBT during turn-on. According to (3) and (4) the di_C/dt and dv_{CE}/dt of IGBT can be controlled by adjusting the gate resistance of IGBT which in turn can be controlled by modulating the optical intensity through the OTPT which is placed in the charging path of the gate.

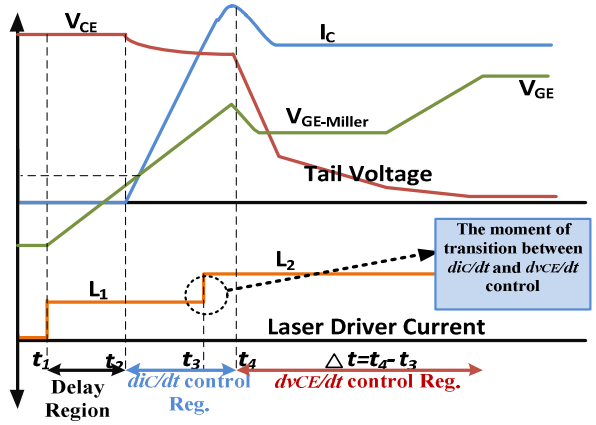

Fig. 21: Key waveforms of turn-on behavior of an IGBT.

The standard clamped-inductive test circuit and control block diagram for optical transition control are shown in Fig. 22.The test circuit comprises a bridge leg with the hybrid device package (comprising M1 and the two OTPTs) placed in the low side and a self-gated IG PSD (M2) in the high side. M1and M2 can be either MOSFET or IGBT. OTPT1 and OTPT2 work complementarily and turn the M1 on and off, respectively. V_1 and V_2, respectively, dictate the turn-on di_C/dt and dv_{CE}/dt of M1 by controlling the current passing through the laser1. The current through the laser1 controls the optical intensity which is emitted to OTPT1 and indirectly controls the gate resistance of M1 during turn-on. Similarly voltages V'_1 and V'_2, respectively, control the turn-off dv_{DS}/dt and di_D/dt of M1 through adjusting the current passes through the laser2.

During the turn-off transition for MOSFET v_{DS} and dv_{DS}/dt are sensed using sensing circuits. Then they are fed to the control circuit. Because of the Δt seconds delay in the OTPT and feedback-loop control circuit predicts the onset of transition from the dv_{DS}/dt to di_D/dt control region and initiates the transition in Δt seconds prior the start of di_D/dt control region by changing the current of the laser-driver2 from a value corresponding to V'_1 to another value corresponding to V'_2. Similarly, during the turn-on transition for IGBT, di_C/dt is sensed and fed to the control circuit. Control circuit predicts the onset of transition from di_C/dt to dv_{CE}/dt control region by changing the current of the laser-driver1 from a value corresponding to V_1 to another value corresponding to V_2.

The complete circuit set up in Fig. 23 is designed and fabricated following Fig. 22. This design includes power circuit and control circuit as well as laser driver and laser in a single board.

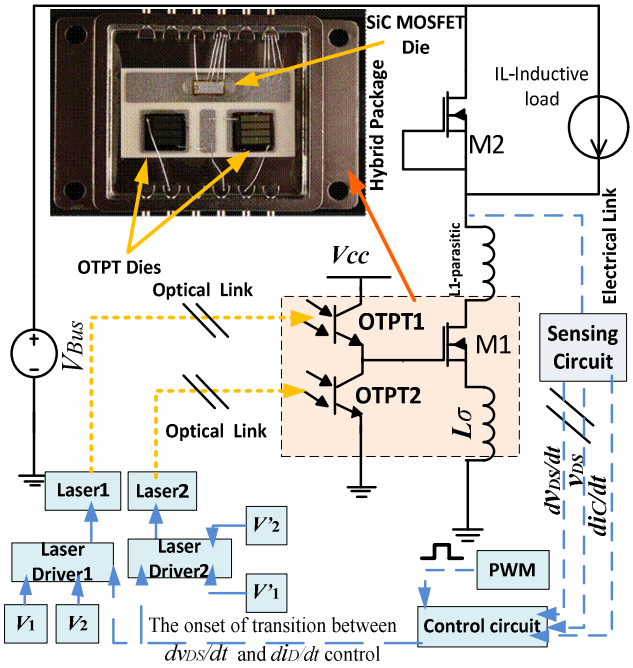

Fig. 22: Test circuit and control block diagram.

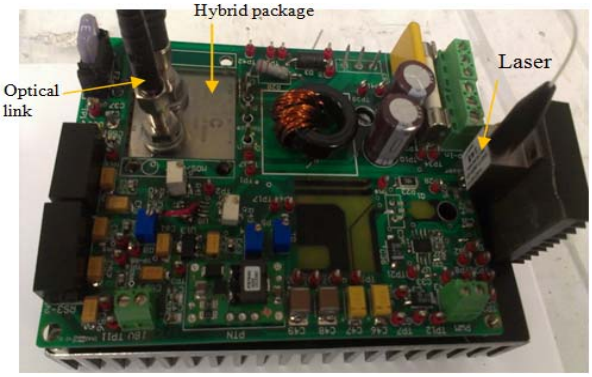

Fig. 23: Fabricated board, which includes power circuit, control circuit, laser, and laser driver [8], [9].

The turn-off drain-to-source voltage (v_{DS}) of M1, and current of laser driver for the cases of conventional gate drive and proposed optical controller are, respectively, found in Fig. 24 and Fig. 25. It has been shown that by reducing the current of the laser driver (which increase

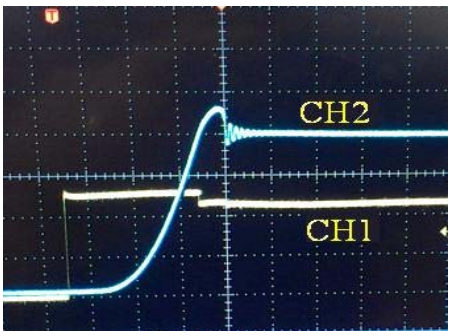

Fig. 24: Turn off behavior of conventional gate drive. CH1: laser driver current, 1 A/div; CH2: drain-source voltage, 100 V/div; time division: 200 nsec/div.

the resistance of OTPT2) in optical controller, the overvoltage and oscillation of v_{DS} lessens comparing to the conventional gate driver. This is because of reduction of di_C/dt in the di_C/dt control region.

Experimental results of turn-on optical control of M1 (which is IGBT in this case) are shown in Fig. 26. In this case the current of the laser driver is fixed in the dv_{CE}/dt control region. As the result, the dv_{CE}/dt is similar for all the cases. On the other hand, as the di_C/dt is decreased in the di_C/dt control region the reverse-recovery current lessens.

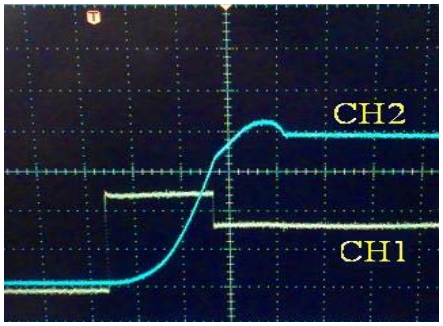

Fig. 25: Turn off behavior with the proposed control. CH1: laser driver current, 1 A/div; CH2: Drain-source voltage, 100 V/div; time division: 200 nsec/div.

Experimental results of turn-on optical control of M1 (which is IGBT in this case) are shown in Fig. 26. In this case the current of the laser driver is fixed in the dv_{CE}/dt control region. As the result, the dv_{CE}/dt is similar for all the cases. On the other hand, as the di_C/dt is decreased in the di_C/dt control region the reverse-recovery current lessens.

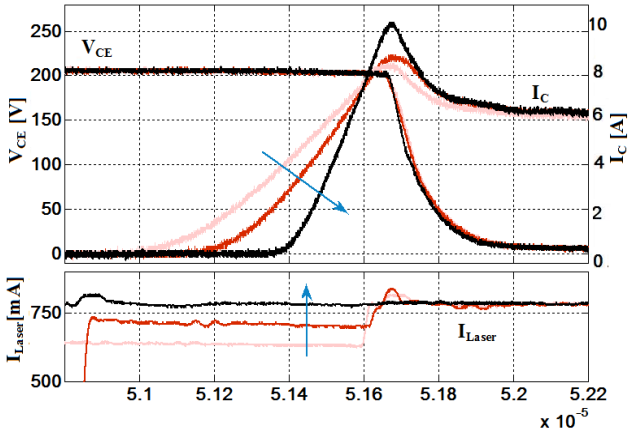

Fig. 26: Measured turn-on waveforms of v_{CE}, i_C and I_{Laser} with the varied current slope (di_C/dt) and fixed voltage slope (dv_{CE}/dt).

V. Summary and Conclusions

In this paper, an overview of the work related to optically-triggered power semiconductor devices and switching transition control have been outlined. With regard to optical devices, a systematic pathway of progress and feasibility with regard to realization of varied functionality, complexity, and material base have been demonstrated. The transition control using optically-triggered devices have been demonstrated for field-effect as well as bipolar power semiconductor devices along with realization of control mechanism. It appears that optical control provides a relatively simple and yet a robust approach to controlling switching dynamics on the fly that can/will have profound effect on system reliability, efficiency, and dynamic response.

References

[1] S.K. Mazumder and T. Sarkar, 'Optically-activated gate control for power electronics', IEEE Transactions on Power Electronics, vol. 26, no. 10, pp. 2863-2886, 2011.

[2] S.K. Mazumder, T. Sarkar, and S.N. Bose, "Photonic modulation of SiC based power semiconductor device switching dynamics using optically triggered power transistor", Plenary Paper, Int. Workshop on the Physics of Semiconductor Devices, 2009.

[3] R. Singh et al., "Large area, > 8 kV SiC GTO thyristors with innovative gate-anode designs", ICSCRM, 2009.

[4] A. Meyer, A. Mojab, and S.K. Mazumder, "Evaluation of first 10-kV optical ETO thyristor operating without any low-voltage control bias", IEEE International Symposium on Power Electronics for Distributed Generation Systems, 2013.

[5] Q. Zhang, A. Agarwal, C. Capell, L. Cheng, M. O'Loughlin, A. Burk, J. Palmour, V. Temple, A. Ogunniyi, H. O'Brien, and C.J. Scozzie, "SiC super GTO thyristor technology development: Present status and future perspective," Pulsed Power Conference (PPC), pp. 1530-1535, Jun. 2011.

[6] S.K. Mazumder, "Photonically activated single bias fast switching integrated thyristor," U.S. Patent Appl. No. 13/281,207, filed in Oct. 2011.

[7] A. Meyer; S. K. Mazumder; H. Riazmontazer, "Optical control of 1200-V and 20-A SiC MOSFET," Applied Power Electronics Conference and Exposition (APEC), 2012 Twenty-Seventh Annual IEEE, vol., no., pp.2530, 2533, 5-9 Feb. 2012.

[8] H. Riazmontazer and S.K. Mazumder, "Dynamic optical turn off control of a high voltage SiC MOSFET, IEEE Applied Power Electronics Conference and Exposition, pp. 1274-1278, 2013.

[9] H. Riazmontazer and S.K. Mazumder, "Optically-switched-drive based unified independent dv/dt and di/dt control for turn-off transition of power MOSFETs", accepted, IEEE Transactions on Power Electronics, 2014.